USCAP

www.nature.com/labinvest

ARTICLE

Check for updates

Exosomes derived from hypoxia-induced alveolar epithelial cells stimulate interstitial pulmonary fibrosis through a HOTAIRM1-dependent mechanism

Lin Chen[1,2], Yang Yang[1,2], Ruiming Yue[2,3], Xiaying Peng[1,2], Hua Yu[2,4] and XiaoBo Huang[2,3]✉

Pulmonary fibrosis is the result of various diseases with no satisfactory treatment approaches. The exosome-mediated transfer of long noncoding RNAs (lncRNAs) has been implicated in the pathological process of lung diseases. Herein, we investigated the therapeutic potential of HOTAIRM1 transferred by alveolar epithelial cell (AEC)-derived exosomes in interstitial pulmonary fibrosis (IPF) and the potential molecular mechanisms. Next-generation sequencing-based gene expression profiling was employed to identify lncRNAs related to IPF. Exosomes were isolated from hypoxia-induced AECs (AEC-exosomes) and identified before use. HOTAIRM1 expression was examined in bleomycin-induced IPF mouse models and the isolated exosomes, and the miRNA downstream of HOTAIRM1 was analyzed. HOTAIRM1 expression was increased in the lung tissues of IPF mice and AEC exosomes. HOTAIRM1 delivered by AEC-exosomes promoted the proliferation and transdifferentiation of lung fibroblasts (LFs). Mechanistically, HOTAIRM1 competitively bound to miR-30d-3p and recruited YY1 to upregulate HSF1 expression. In addition, miR-30d-3p targeted HSF1 by binding to its 3′-UTR and reduced its expression. In vivo assays confirmed the promoting effect of exosomes-HOTAIRM1 on extracellular matrix remodeling by regulating the miR-30d-3p/HSF1/YY1 axis. Overall, HOTAIRM1 loaded by AEC exosomes can accelerate IPF by disrupting miR-30d-3p-mediated inhibition of HSF1 and inducing recruitment of HSF1 by YY1. These results highlight a promising strategy to overcome IPF.

Laboratory Investigation (2022) 102:935–944; https://doi.org/10.1038/s41374-022-00782-y

INTRODUCTION

Interstitial lung disease, a battery of diffuse parenchymal lung disorders, contributes to increased morbidity and mortality [1]. Most types of interstitial lung disease can develop into extensive fibrosis [2]. Pulmonary fibrosis is caused by aberrant wound healing, which results in a chronic inflammatory response and excessive accumulation of extracellular matrix components [3, 4]. This disease is ascribed to many etiologies, including genetic defects, autoimmune diseases and environmental exposures, and upon development, it is irreversible and most often progressive [5]. Uncovering the potential early-detection molecular markers underlying the pathogenesis of interstitial pulmonary fibrosis (IPF) will thus be critical to reduce its frequency.

Exosomes are small vesicles (30–200 nm in diameter) with a single membrane that are enriched in proteins, lipids, nucleic acids, etc., and show cell-like topology [6]. Exosomal long noncoding RNAs (lncRNAs) have appealing value for clinical application in the diagnosis, prognosis, and treatment of lung diseases, including pulmonary fibrosis [7]. LncRNAs are a type of noncoding RNA that comprise sequences longer than 200 nucleotides, the expression of which is evidently altered in fibrotic lung tissues, serving as potential molecular targets for inhibiting the development of pulmonary fibrosis [8, 9]. The lncRNA HOXA transcript antisense RNA myeloid specific 1 (HOTAIRM1), which is highly expressed in non-small-cell lung cancer (NSCLC), may be a promising diagnostic and prognostic biomarker for NSCLC due to its association with poor prognosis and clinicopathologic grading [10]. However, its potential role in IPF remains elusive. The LncBase and miRWalk databases employed in the current study provided information on the binding affinity between HOTAIRM1 and microRNA (miR)-30d-3p. Inhibition of miR-30 by cadmium, a known human lung carcinogen, in human lung epithelial cells can contribute to many lung diseases, such as chronic obstructive pulmonary disease and fibrosis [11]. Published data have suggested that the overexpression of miR-30a abrogates the pro-autophagic effects of Yin-Yang 1 (YY1) in pancreatic cancer cells [12]. The enhanced expression of YY1 can promote the profibrotic phenotype in primary alveolar epithelial cells (AECs) and thereby accelerate pulmonary fibrosis progression [13]. YY1 has been shown to directly activate the transcription of HSF1 in the context of breast cancer [14]. Meanwhile, the downregulation of HSF1 leads to the repression of the proliferative ability and the fibrogenic transformation of human embryonic pulmonary fibroblasts and thus prevents IPF [15]. We thus designed this

[1]Department of Respiratory and Critical Care Medicine, Sichuan Provincial People's Hospital, University of Electronic Science and Technology of China, Chengdu 610072, P. R. China. [2]Chinese Academy of Sciences Sichuan Translational Medicine Research Hospital, Chengdu 610072, P. R. China. [3]Department of Critical Care Medicine, Sichuan Provincial People's Hospital, University of Electronic Science and Technology of China, Chengdu 610072, P. R. China. [4]Department Laboratory Medicine, Sichuan Provincial People's Hospital, University of Electronic Science and Technology of China, Chengdu 610072, P. R. China. ✉email: huangxiaobo@med.uestc.edu.cn

Received: 23 July 2021 Revised: 14 March 2022 Accepted: 22 March 2022
Published online: 27 April 2022

study to examine the role of HOTAIRM1 shuttled by hypoxia-induced AEC-derived exosomes (AEC-exosomes) in IPF progression and its association with miR-30d-3p, YY1 and HSF1.

MATERIALS AND METHODS

Ethics statement

This study was performed with the approval of the Animal Ethics Committee of Sichuan Provincial People's Hospital (2019047 A) and conformed to the Guide for the Care and Use of Laboratory Animals of the National Institutes of Health. Extensive efforts were made to minimize animal suffering.

Next-generation sequencing (NGS)-based gene expression profiling

The FPKM data of the RNA-Seq dataset GSE124685 were downloaded from the Gene Expression Omnibus (GEO) database, which consisted of 35 normal samples and 49 IPF samples. After replacing the repeated probes in the matrix with the average value using the R language "limma" package, the Wilcoxon method was utilized to identify differentially expressed genes in IPF with $|\log FC| > 2$ and p value < 0.05 set as the threshold. The RNAInter database was adopted for RNA–protein interaction analysis. The GEPIA database was applied to analyze the correlation of gene expression in lung tissues in GTEx. The miRNAs bound by lncRNAs and mRNAs were predicted using the LncBase and miRWalk databases.

IPF mouse model construction

Male C57BL/6 mice (weighing 23–25 g, aged 6–8 weeks; Experimental Animal Center of the Shanghai Institute of Materia Medica, Chinese Academy of Sciences, Shanghai, China) were fed fine pellets and given *ad libitum* access to water at 22 ± 1 °C with a 12-h light/dark cycle. The mice were acclimated for one week and then randomly divided into a normal group ($n = 6$) and an IPF group ($n = 48$). The IPF mice were anesthetized with 100 mg/kg sodium pentobarbital and intratracheally injected with bleomycin (50 mg/kg per mouse in 50 μL of normal saline; Zhejiang Hisun Pharmaceutical Co., Ltd., Taizhou, China). Lung function was assayed by resistance and compliance plethysmographs (Yuyan Instruments, China) after 2 weeks. Lung compliance was decreased significantly, while lung resistance was increased, indicating the successful construction of IPF models. The normal mice were intratracheally administered with the same amount of normal saline.

Forty-eight IPF mice were then randomly treated with lv-oe-NC (injected with lentivirus carrying oe-NC), lv-oe-HOTAIRM1 (injected with lentivirus carrying oe-HOTAIRM1), lv-sh-NC (injected with lentivirus carrying sh-NC), lv-sh-HOTAIRM1 (injected with lentivirus carrying sh-HOTAIRM1), exosomes-oe-NC + sh-NC (treated with exosomes from oe-NC-transfected AECs and injected with lentivirus carrying sh-NC), exosomes-oe-HOTAIRM1 + sh-NC (treated with exosomes from oe-HOTAIRM1-transfected AECs and injected with lentivirus carrying sh-NC) and exosomes-oe-HOTAIRM1 + sh-HSF1 (treated with exosomes from oe-HOTAIRM1-transfected AECs and injected with lentivirus carrying sh-HSF1). The titer of the lentiviral particles was 1×10^9 TU/mL (all lentiviral particles were sourced from Genechem., Shanghai, China). On the 5th day of bleomycin induction and afterward, lentivirus was delivered into the mice *via* the tail vein, with 200 μL of normal saline or exosomes delivered *via* the tail vein every 4 days. Three weeks later, the lung tissue was harvested from the mice after euthanasia, fixed with 4% paraformaldehyde, and embedded in paraffin for subsequent experiments. A portion of the lung tissue was stored in liquid nitrogen for later use.

Hematoxylin-eosin (HE) staining

After fixation, lung tissues embedded in paraffin were sectioned using an automatic microtome (RM2265, Beijing Changheng Rongchuang Technology Co., Ltd., Beijing, China). Following dewaxing and rehydration, the sections were dyed according to the specifications of the HE staining kit (Nanjing Shenghang Biotechnology Co., Ltd., Nanjing, China, BC-DL-001–100 mL) before observation under an optical microscope (Eclipse E200, Shanghai Fenye Photoelectric Equipment Co., Ltd., Shanghai, China). Lung tissue edema, inflammatory cell infiltration, hemorrhage and cell necrosis were evaluated in a double-blind manner by two pathologists.

Masson's trichrome staining

The pretreatment of the sections was the same as that for HE staining. The sections were dyed in compliance with the instructions of the Masson's trichrome staining kit (Solarbio, Beijing, China). The staining results showed collagen fibers as blue. An optical microscope (Eclipse E200, Fenye Photoelectric Equipment) was used for visualization, and ImageJ software was adopted for quantification.

Immunohistochemistry

Initially, 4-μm-thick paraffin sections were dewaxed, hydrated and washed, followed by endogenous peroxidase neutralization and antigen retrieval. Next, goat serum (C-0005, Shanghai Haoran Biotechnology Co., Ltd., Shanghai, China) was utilized for blocking the activity of peroxidase at 37 °C for 1 h and probed overnight at 4 °C with primary rabbit antibodies against α-SMA (1:50, ab5694, Abcam, UK), collagen I (1:500, ab270993, Abcam), fibronectin (1:100, PA5-29578, Thermo Fisher Scientific, Waltham, MA, USA), and Vimentin (1:200, ab92547, Abcam). The following day, anti-IgG (ab172730, Abcam) served as the secondary antibody for reprobing. Following PBS washing, the sections were treated with a two-step assay kit (PV-9000, Beijing Nobleryder Technology Co., Ltd., Beijing, China), developed with a DAB kit (C520017, Shanghai Sangon Biotechnology Co., Ltd., Shanghai, China), counterstained with hematoxylin (PT001, Shanghai Bogoo Biological Technology Co., Ltd., Shanghai, China), dried at 65 °C and sealed. Finally, microscopic images were captured under an upright microscope (BX63, Fujian Chuangpu Technology Co., Ltd., Fujian, China) in 5 high-power fields chosen at randomization from each section and quantified using ImageJ software.

Determination of hydroxyproline

The fresh lung tissues were dried at 100 °C for at least 24 h, hydrolyzed utilizing 0.5 μM acetic acid and 0.1 mg/mL pepsin under hypoxia, sealed in vacuum bottles, and hydrolyzed again at 4 °C. On the second day, a hydroxyproline test kit (A030-1-1) offered by JianCheng Bioengineering Institute (Nanjing, China) was used to evaluate the level of hydroxyproline in lung tissues.

Cell culture

The mouse AEC line MLE12 (C2008, Yingwan Biotechnology, Shanghai, China) was cultured with Roswell Park Memorial Institute (RPMI) 1640 medium (11875101, Thermo Fisher Scientific) supplemented with 10% fetal bovine serum (FBS), 50 U/mL penicillin, and 50 U/mL streptomycin in an incubator containing 5% CO_2 at 37 °C. For hypoxic exposure, the MLE12 cell line was incubated for 4 h in serum-free medium containing 1% O_2, 95% N_2, and 5% CO_2. Then, the cells were cultured for 24 h in a normoxic (21% O_2) environment.

Culture of mouse primary lung fibroblasts (LFs): The lung tissues obtained from 6- to 8-week-old C57BL/6 mice were minced into 1-mm^3 pieces. The pieces were immersed in digestion buffer (Sigma) supplemented with 30 mg of collagenase IV, 1 g of FBS, 96 mL of Hank's buffer solution, and 4 mL of 0.25% trypsin. After 1 h, the strained tissue suspension was centrifuged at 300 g and 4 °C for 5 min. The pellet was resuspended in DMEM (D0819, Shanghai Sigma–Aldrich Trading Co., Ltd., Shanghai, China), followed by another 5 min of centrifugation at 500 g and 4 °C and 5 min of at 300 g and 4 °C. The harvested cells were identified as LFs by vimentin immunohistochemical staining and finally cultured at 37 °C in an incubator containing 5% CO_2.

Isolation and identification of exosomes

In a 10-cm culture dish, AECs cultured under normoxia and hypoxia were cultured in exosome-free serum medium (centrifugation at 120,000 × *g* and 4 °C, 14 h) for 72 h. When the cells reached 90–100% confluence, the culture medium was centrifuged at 3000 ×g and 4 °C for 10 min to remove the cells. Subsequently, another centrifugation (10,000 × *g*) was performed at 4 °C for 30 min to remove dead cells and debris. The supernatant was harvested and filtered through a 0.22-μm filter (SLGV033RB, Solarbio) to remove the smaller cell debris, followed by ultracentrifugation at 100,000 × *g* and 4 °C for 2 h using Optima L-80XP (Shanghai Aiyan Biotechnology Co., Ltd., Shanghai, China). Following supernatant removal, the pellet suspension (prepared in 70 mL of ice-cold PBS) was ultracentrifuged at 100,000 × *g* and 4 °C for 2 h. The PBS was carefully discarded, and the pellet was purified using a kit and resuspended in PBS. Thereafter, a second ultracentrifugation was conducted under the same conditions,

and the precipitate was cryopreserved (−80 °C) for later use or immediate use.

The morphological observation of the isolated exosomes was implemented utilizing a Hitachi H-7650 transmission electron microscope (TEM; Hitachi Chemical, Tokyo, Japan). A NanoSight nanoparticle tracking analyzer (ZetaView_Particle Metrix, DKSH, China) was utilized to measure the size distribution of the exosomes. The expression of exosome surface markers (CD63 [1:3000, rabbit, ab134045, Abcam], TSG101 [1:1000, rabbit, ab125011, Abcam] and GM130 [1:500, rabbit, PA1-077, Thermo Fisher Scientific]) was measured by Western blot analysis.

Uptake of exosomes by LFs

AECs transiently transfected with Cy3-labeled HOTAIRM1 (Cy3-HOTAIRM1, 1.2×10^6) were placed in the lower chamber of the coculture chamber, and 1×10^6 LFs were added to the upper chamber. After 24 h of coculture, Cy3 fluorescence in the LFs was observed with a fluorescence microscope. AECs-HOTAIRM1-Cy3 exosomes were incubated with LFs at 37 °C for 12 h. The cells were fixed with 4% paraformaldehyde, washed with PBS, and dyed with DAPI (P36931, Thermo Fisher Scientific). A confocal microscope (Zeiss LSM 800, Beijing Opton Optical Technology Co., Ltd., Beijing, China) was utilized to observe the uptake of labeled EVs by LFs. Five images were captured at random for each sample.

Cell treatment

LFs at the logarithmic growth phase were detached with 0.25% trypsin, seeded in a 6-well plate, 1×10^5 cells/well, and cultured for 24 h. Upon reaching 60–75% confluence, the cells were exposed to 10 μM MG132 (protease inhibitor, M7449, Sigma–Aldrich) and then transfected using Lipofectamine 2000 reagent (11668019, Thermo Fisher Scientific) with plasmids of oe-NC, oe-HOTAIRM1, sh-NC, sh-HOTAIRM1, oe-NC + mimic NC, oe-HOTAIRM1 + mimic NC, oe-HOTAIRM1 + miR-30d-3p mimic, oe-NC + sh-NC, oe-HOTAIRM1 + sh-NC, oe-HOTAIRM1 + sh-YY1, miR-30d-3p mimic, miR-30d-3p inhibitor, oe-YY1, sh-YY1#1, sh-YY1#2, sh-HSF1#1, sh-HSF1#2, mimic NC + oe-NC, miR-30d-3p mimic + oe-NC, miR-30d-3p mimic + oe-HSF1, oe-YY1 + sh-NC and oe-YY1 + sh-HSF1. These plasmids were purchased from and synthesized by Shanghai Genechem Co., Ltd. (Shanghai, China). The medium was changed after 6 h to continue the culture. After 48 h, the cells were used for subsequent experiments.

RNA isolation and quantitation

Total RNA was extracted from cells or tissues using TRIzol reagent (10296010, Thermo Fisher Scientific). The concentration and purity of total RNA were determined using a NanoDrop™ Lite spectrophotometer (ND-LITE, Thermo Fisher Scientific). Total RNA was reverse transcribed into complementary DNA (cDNA) with the TaqMan™ MicroRNA Reverse Transcription Kit (4366597, Thermo Fisher Scientific), PrimeScript RT Kit (RR047A, Wuhan Khayal Bio-Technology Co., Ltd., Hubei, China) and MiRCURY-LNA-miRNA-PCR Kit (339306, Future Biotech, Beijing, China). RT–qPCR was conducted using the Applied Biosystems QuantStudio system (Shanghai Jianling Information Technology Co., Ltd., Shanghai, China). U6 served as the loading control for miRNA, and GAPDH served as the loading control for the remaining genes. The primers were designed by Sangon, and the sequences are listed in Table S1. Fold changes were calculated employing the relative quantification ($2^{-\Delta\Delta Ct}$) method.

Western blot analysis

Total protein was extracted from tissues or cells utilizing radioimmunoprecipitation assay lysis buffer with 1% protease inhibitor, with the concentration assayed by a bicinchoninic acid kit (A53226, Thermo Fisher Scientific). Next, protein was separated using 10% sodium dodecyl sulfate–polyacrylamide gel electrophoresis and transferred onto polyvinylidene fluoride membranes. The membranes were then blocked using 5% skimmed milk powder at ambient temperature for 1 h and underwent overnight incubation at 4 °C with primary rabbit antibodies against α-SMA (1 μg/mL, ab5694, Abcam), collagen I (1:1000, ab270993, Abcam), fibronectin (1:1000, PA5-29578, Thermo Fisher Scientific), PCNA (1 μg/mL, PA5-32541, Thermo Fisher Scientific), and β-actin (#8457, 1:1000, Cell Signaling Technologies [CST], Beverly, MA, USA, serving as a loading control). The next day, the secondary antibody horseradish peroxidase-tagged goat anti-rabbit IgG (#7074, 1:2000, CST) was added for 1 h of incubation. The membranes were developed, and band intensities were quantified using ImageJ 1.48 software.

Chromatin immunoprecipitation (ChIP)

ChIP assays were conducted according to the manufacturer's instructions for the ChIP Kit (P2078, Beyotime). LFs transfected with YY1 were fixed with 1% formaldehyde solution for 10 min to produce DNA–protein cross-linking, which was terminated by incubation with 1.1 mL of glycine for 5 min. The sample was lysed in lysis buffer and sonicated to obtain 200–1000 bp chromatin fragments. Afterward, 10 μL of the supernatant was used as input, and the DNA–protein complex was probed with anti-YY1 antibody (2.5 μg/10^6 cells, PA5–29171, Thermo Fisher Scientific) or NC IgG (#7074, 1:2000, CST) at 4 °C overnight. After immunoprecipitation, the chromatin was decrosslinked at 65 °C for 4 h, and the DNA was purified, followed by RT–qPCR detection. The HSF1 sequence is presented in Table S1.

Fluorescence in situ hybridization (FISH)

The Cy3-labeled HOTAIRM1 probe and FITC-labeled miR-30d-3p/YY1 probe were sourced from Geneseed Biotech Co., Ltd. (Guangzhou, China). Primary LFs were grown on round coverslips, followed by fixation in PBS containing 0.5% Triton X-100 and dehydration. The FISH probe was diluted (1:50), denatured, equilibrated, and added to the cells overnight incubation at 37 °C. After hybridization, the cells were labeled with DAPI-Antifade for 10 min, and the glass slide was sealed with a rubber adhesive and maintained in the dark for over 20 min. Finally, a TCS SP8 X laser confocal microscope system (88211109, Beijing Image Trading Co., Ltd., Beijing, China) was used to observe localization.

Dual-luciferase reporter assay

The 3′-UTR sequence of HOTAIRM1 carrying the putative miR-30d-3p binding site or the mutated binding site was inserted into the pGL3-basic vector (6107, Shanghai Jiran Biotechnology Co., Ltd., Shanghai, China), with the HOTAIRM1-3′-UTR-wild type (WT) (5′-ACUGAA-3′), HSF1-3′-UTR-WT (5′-ACUGAA-3′), HOTAIRM1-3′-UTR-mutant (MUT) (5′-TGACTT-3′) and HSF1-3′-UTR-MUT (5′-TGACTT-3′) obtained. HEK-293T cells were seeded in a 24-well plate and incubated for 24 h. Upon reaching 50–60% confluence, the cells were manipulated with the aforementioned reporter plasmids and mimic NC or miR-30d-3p mimic in combination using Lipofectamine 2000 reagent. In addition, 10 ng of pRL-TK Renilla luciferase served as a control. After 24 h, luciferase activity detection was performed with the Dual-Luciferase Reporter Gene Assay System (Shenzhen Tuopu Biotechnology Co., Ltd., Shenzhen, China), and Renilla luciferase activity was used for normalization.

Cell counting kit-8 (CCK-8) assay

LFs in a 96-well plate (5×10^3 cells/well) were incubated with 10 μL/well of CCK-8 solution (Beyotime) in a humidified incubator at 37 °C for 1 h, and the optical density (OD) value was recorded at 450 nm using a microplate reader (abx700005, QiWei YiCheng Tech Co., Ltd., Beijing, China).

Immunofluorescence

LFs were fixed in 4% paraformaldehyde for 30 min, permeated, and blocked at ambient temperature. The incubation of cells with antibodies was conducted at 4 °C overnight. The antibodies contained α-SMA (#19245, 1:200, CST), HSF1 (rabbit, 1:200, ab76076, Abcam), collagen I (ab260043, 1:200, Abcam), fibronectin (ab2413, 1:200, Abcam), Ki67 (rabbit, 1:100, ab15580, Abcam) and PCNA (rabbit, 1:500, ab18197, Abcam). Following washing, the cells were incubated with Alexa Fluor® 555-coupled goat anti-rabbit (#60839, 1:50, CST) in the dark. Nuclear staining with DAPI (Roche Molecular Biochemicals, Basel, Switzerland) lasted for 5 min. Finally, the cells were observed under a fluorescence microscope (80i, Shanghai Henghao Instruments Co., Ltd., Shanghai, China), and fluorescence quantitative analysis was performed using ImagePro Plus software.

Statistical analysis

All data were analyzed using GraphPad Prism 8.0 (GraphPad Software, La Jolla, CA, USA). The experiment was conducted three times independently. The measurement data are described as the mean ± standard deviation. Data between two groups were compared by unpaired *t test*. Differences among multiple groups were statistically analyzed employing one-way analysis of variance (ANOVA) and Tukey's multiple comparisons test. Statistical analysis in relation to time-based measurements within each group was realized using two-way ANOVA or repeated-measures ANOVA,

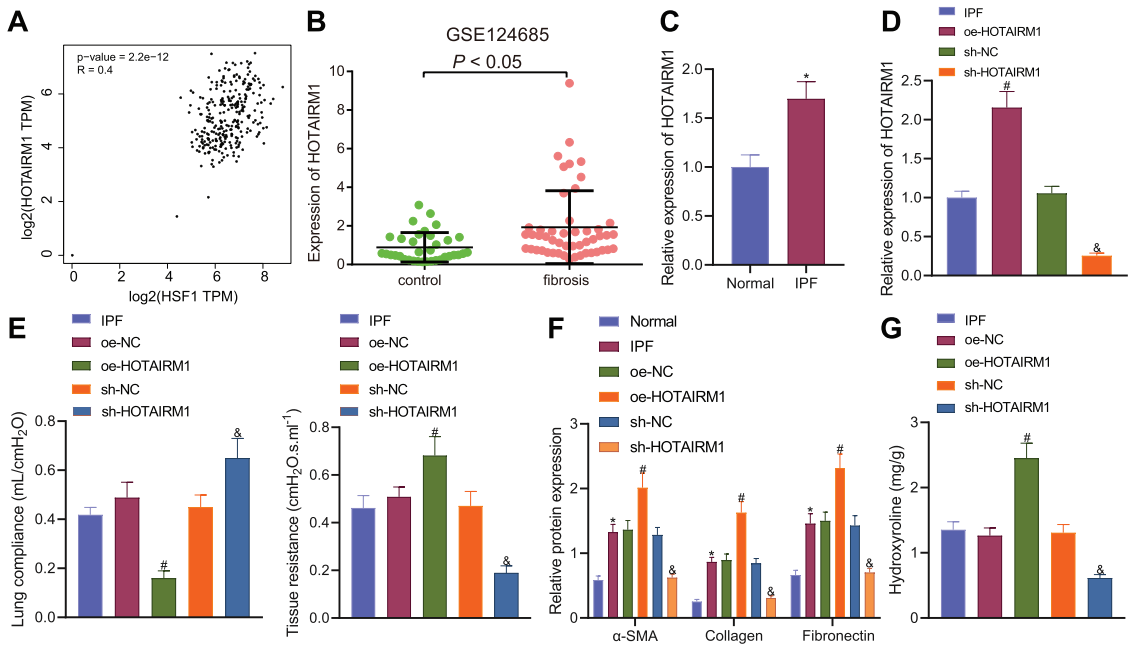

Fig. 1 HOTAIRM1 is increased in lung tissues of IPF mice and initiates IPF. A Correlation between the expression of HOTAIRM1 and HSF1 in lung tissues in GTEx in the GEPIA database. **B** HOTAIRM1 expression in normal ($n = 35$) and IPF samples ($n = 49$) in the GSE124685 dataset. **C** RT–qPCR detection of HOTAIRM1 expression in lung tissues of normal ($n = 6$) and IPF mice ($n = 6$). **D** RT–qPCR detection of HOTAIRM1 expression in lung tissues of IPF mice treated with oe-HOTAIRM1 or sh-HOTAIRM1. **E** Lung compliance and resistance in lung tissues of normal mice and IPF mice treated with oe-HOTAIRM1 or sh-HOTAIRM1. **F** Western blot analysis of α-SMA, collagen I, and fibronectin proteins in lung tissues of IPF mice treated with oe-HOTAIRM1 or sh-HOTAIRM1. **G** Level of hydroxyproline in the lung tissue of IPF mice treated with oe-HOTAIRM1 or sh-HOTAIRM1. $n = 6$ for mice upon each treatment. The data are shown as the mean ± standard deviation. Data between two groups were analyzed by unpaired *t test*, while those among multiple groups were assessed by one-way ANOVA with Tukey's post-hoc tests. $^{*}p < 0.05$, compared with normal mice. $^{\#}p < 0.05$, compared with oe-NC-treated mice. $^{\&}p < 0.05$, compared with sh-NC-treated mice.

followed by Tukey's post-hoc test for multiple comparisons. A value of $p < 0.05$ was considered significant.

RESULTS

HOTAIRM1 is highly expressed in IPF and promotes IPF progression

We first performed GEPIA database analysis and found that HOTAIRM1 expression was positively correlated with that of HSF1 in lung tissues in GTEx, with an r value of +0.4 (Fig. 1A). Analysis of the GSE124685 dataset revealed that more HOTAIRM1 was produced by cells in IPF samples than in normal samples (Fig. 1B).

In the established IPF mouse model, lung compliance was reduced, while lung resistance was enhanced (Supplementary Fig. 1), indicating successful IPF mouse model construction. RT–qPCR data revealed an increased level of HOTAIRM1 in the lung tissues of IPF mice compared with normal mice (Fig. 1C). Therefore, we speculate that HOTAIRM1 may be the key lncRNA that affects the occurrence of IPF.

For verification, gain- and loss-of-function tests were first conducted, and the results showed that treatment with lentivirus carrying oe-HOTAIRM1 upregulated HOTAIRM1 expression, while lentivirus carrying sh-HOTAIRM1 decreased its expression in the lung tissue of IPF mice (Fig. 1D). In addition, HOTAIRM1 overexpression reduced lung compliance and increased lung resistance, but the silencing of HOTAIRM1 led to the opposite results (Fig. 1E). HE and Masson's trichrome staining indicated obvious inflammatory cell infiltration, capillary hyperplasia, increased collagen fiber bundles, and enhancement of lung fibrosis in the lung tissues of IPF mice. Moreover, in the presence of HOTAIRM1 overexpression, lung tissue pathology and fibrosis were more obvious, which was negated following the silencing of HOTAIRM1 (Supplementary Fig. 2A, B).

In addition, the results of immunohistochemistry (Supplementary Fig. 2C) and Western blot analysis (Fig. 1F) of fibrosis-related proteins revealed higher expression of α-SMA, collagen I and fibronectin in the lung tissue of IPF mice than in normal mice; a more pronounced increase was noted in response to HOTAIRM1 overexpression. Conversely, a decline was induced following the silencing of HOTAIRM1. Furthermore, the level of hydroxyproline in the mouse lung tissues was increased upon HOTAIRM1 elevation, while it was reduced in the absence of HOTAIRM1 (Fig. 1G). Overall, HOTAIRM1 may be upregulated in the lung tissues of IPF mice and could potentially contribute to the development and progression of IPF.

HOTAIRM1, which is enriched in exosomes from hypoxia-treated AECs, promotes IPF progression

We isolated and identified exosomes from AECs. Under TEM, exosomes had a representative double-layer membrane structure with a diameter distribution of approximately 110 nm (Fig. 2A, B). Western blot analysis further showed that CD63 and TSG101 proteins were enriched in the isolated exosomes, while NC GM130 was absent (Fig. 2C), indicating the successful isolation of exosomes.

Western blot analysis showed that hypoxia increased the release of exosomes from AECs (Fig. 2D), and HOTAIRM1 expression was higher in AECs and exosomes under hypoxic conditions than under normoxic conditions (Fig. 2E). The above results demonstrated that hypoxia could induce AECs to release more exosomes with more HOTAIRM1 carried by exosomes.

Coculture data of AECs transiently transfected with Cy3-labeled HOTAIRM1 and LFs suggested the presence of Cy3-labeled green fluorescence in more than 90% of LFs. Similarly, green fluorescence signals were also detected in LFs incubated with AEC-HOTAIRM1-Cy3 exosomes, while the signals were decreased in the

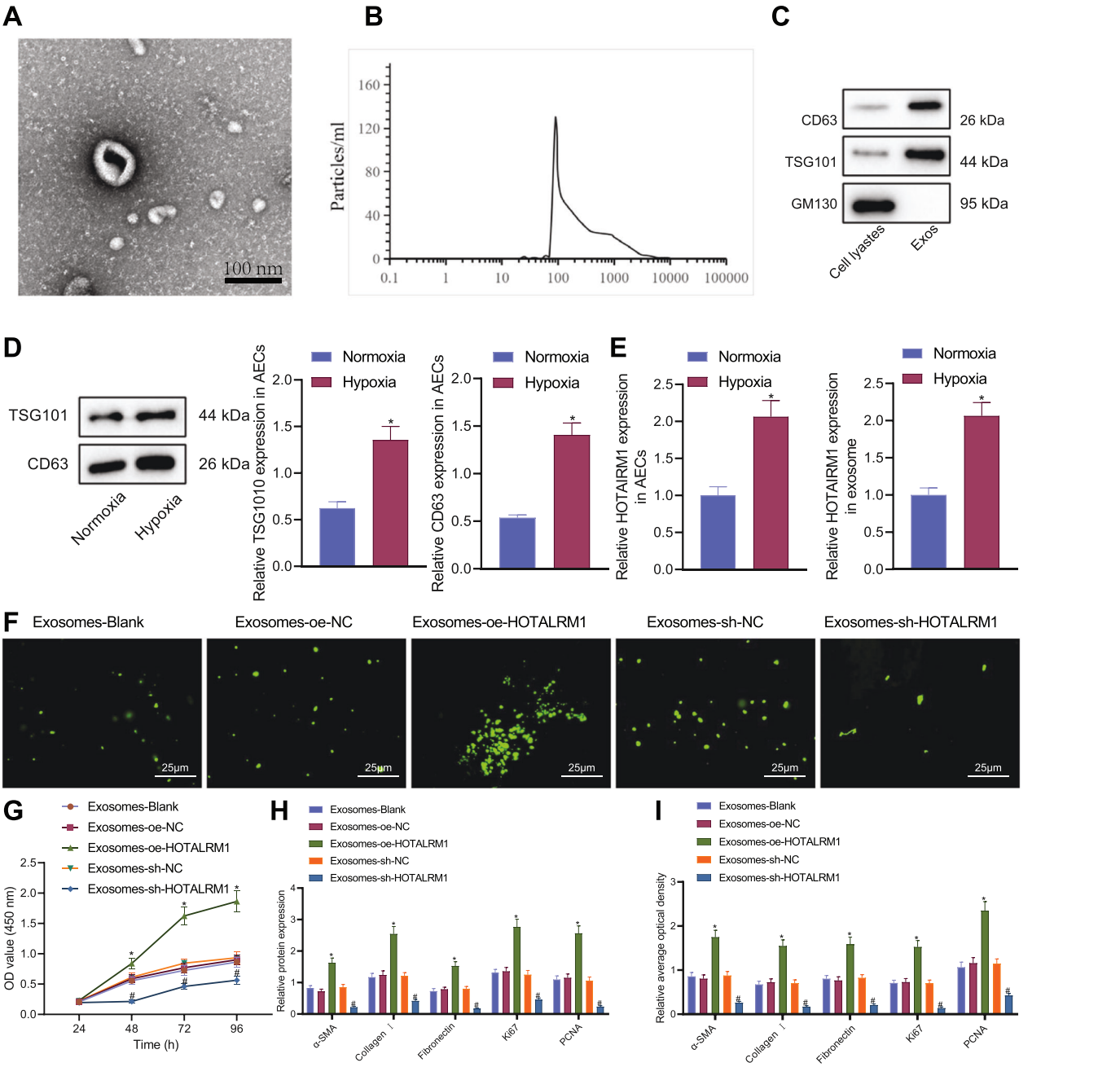

Fig. 2 Exos-HOTAIRM1 stimulates the proliferation and transdifferentiation of LFs. A Morphological characterization of the Exos isolated from hypoxia-induced AECs observed under a TEM (scale bar = 100 nm). **B** Analysis of the size distribution of Exos isolated from hypoxia-treated AECs. **C** Western blot analysis of the Exo marker proteins CD63, TSG101 and GM130 in the Exos. **D** Western blot analysis of CD63 and TSG101 proteins in hypoxia-induced AECs. **E** RT–qPCR detection of HOTAIRM1 expression in hypoxia-induced AECs and Exos. **F** Uptake of AEC-Exos by LFs. **G** CCK-8 detection of the proliferation of LFs cocultured with Exos-oe-HOTAIRM1 or Exos-sh-HOTAIRM1. **H** Western blot analysis of α-SMA, collagen I, fibronectin, Ki67 and PCNA proteins in LFs cocultured with Exos-oe-HOTAIRM1 or Exos-sh-HOTAIRM1. **I** Immunofluorescence analysis of α-SMA, collagen I, fibronectin, Ki67 and PCNA proteins in LFs cocultured with Exos-oe-HOTAIRM1 or Exos-sh-HOTAIRM1. The data are shown as the mean ± standard deviation of three technical replicates. Data between two groups were analyzed by unpaired *t test*, while those among multiple groups were assessed by one-way ANOVA with Tukey's post-hoc tests. Repeated measures ANOVA with Tukey's post-hoc test was applied for the comparison of data at different time points. $^{*}p < 0.05$, compared with normoxia-treated AECs or LFs cocultured with Exos-oe-NC. $^{\#}p < 0.05$, compared with LFs cocultured with Exos-sh-NC.

absence of HOTAIRM1 (Fig. 2F). The aforementioned results indicated that HOTAIRM1 could be delivered to LFs by exosomes secreted by AECs.

CCK-8 data suggested an enhancement in the proliferation of LFs cocultured with exosomes-oe-HOTAIRM1, but a decline was observed in the presence of exosomes-sh-HOTAIRM1 (Fig. 2G). Additionally, higher levels of α-SMA, collagen I, fibronectin, Ki67 and PCNA proteins were noted in LFs cocultured with exosomes-oe-HOTAIRM1 than in LFs cocultured with exosomes-oe-NC. In contrast, these proteins were downregulated in the presence of exosomes-sh-HOTAIRM1 (Fig. 2H, I). Overall, these findings supported that HOTAIRM1 could enter LFs through AEC-exosomes, thereby promoting the proliferation and transdifferentiation of LFs.

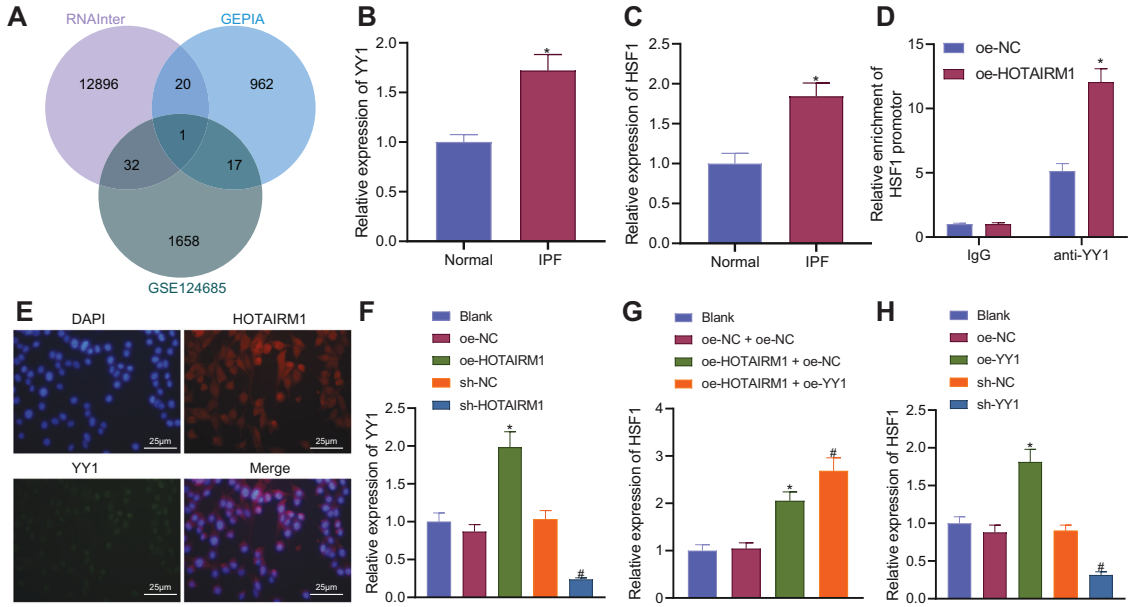

Fig. 3 HOTAIRM1 upregulates HSF1 by recruiting YY1. A Venn diagram of the predicted lncRNAs binding to YY1 by the RNAInter database, HSF1-related lncRNAs in lung tissue in GTEx from the GEPIA database and the differential lncRNAs in the GSE124685 dataset. **B** RT–qPCR detection of YY1 expression in the lung tissues of normal ($n = 6$) and IPF mice ($n = 6$). **C** RT–qPCR detection of HSF1 expression in the lung tissues of normal ($n = 6$) and IPF mice ($n = 6$). **D** Relative enrichment of YY1 in the promoter region of HSF1 measured by ChIP-PCR assay. **E** Subcellular colocalization of HOTAIRM1 and YY1 analyzed by FISH assay. **F** RT–qPCR detection of YY1 expression following treatment with HOTAIRM1 or sh-HOTAIRM1. **G** RT–qPCR detection of HSF1 expression following treatment with oe-HOTAIRM1 or sh-HOTAIRM1. **H** RT–qPCR detection of YY1 expression following treatment with oe-YY1 or sh-YY1. The data are shown as the mean ± standard deviation of three technical replicates. Data between two groups were analyzed by unpaired *t test*, while those among multiple groups were assessed by one-way ANOVA with Tukey's post-hoc tests. $^{*}p < 0.05$, compared with normal mice or treatment with oe-NC or oe-NC + oe-NC. $^{\#}p < 0.05$, compared with treatment with sh-NC or oe-HOTAIRM1 + oe-NC.

HOTAIRM1 recruits YY1 to activate HSF1 expression

We then elucidated the downstream mechanism of HOTAIRM1 in IPF. Venn diagram analysis of the predicted lncRNAs binding to YY1 by the RNAInter database, HSF1-related lncRNAs in lung tissue in GTEx from the GEPIA database and the differential lncRNAs in the GSE124685 dataset indicated that only HOTAIRM1 was found at the intersection (Fig. 3A). RT–qPCR data showed upregulated expression of YY1 and HSF1 in lung tissues sourced from IPF mice (Fig. 3B, C). The results of the ChIP assay displayed an increase in the enrichment of HSF1 in the anti-YY1 group, and the overexpression of HOTAIRM1 enriched additional HSF1 promoters (Fig. 3D). In addition, FISH analysis revealed the colocalization of HOTAIRM1 and YY1 in the nucleus (Fig. 3E). As shown in Fig. 3F, there was an increase in YY1 expression following HOTAIRM1 overexpression, which was abolished by HOTAIRM1 silencing. Manipulation with oe-HOTAIRM1 + oe-NC or oe-HOTAIRM1 + oe-YY1 led to the upregulation of HSF1 expression, with a more obvious upregulation noted following manipulation with oe-HOTAIRM1 + oe-YY1 (Fig. 3G). Furthermore, HSF1 expression was elevated upon YY1 overexpression, whereas a contrary result was observed in the absence of YY1 (Fig. 3H). The above data indicated that HOTAIRM1 could recruit YY1 to elevate the expression of HSF1.

HOTAIRM1 competitively binds to miR-30d-3p and enhances HSF1 expression

The LncBase and miRWalk databases predicted 6 miRNAs that may bind to HOTAIRM1 and HSF1 (Fig. 4A) and predicted the potential binding sites of miR-30d-3p to HOTAIRM1 and HSF1 (Fig. 4B). RT–qPCR indicated reduced expression of miR-30d-3p in the lung tissue of IPF mice compared with that in normal mice (Fig. 4C). Furthermore, manipulation with miR-30d-3p mimic in HEK-293T cells inhibited the luciferase activity of HOTAIRM1-WT without altering that of HOTAIRM1-MUT (Fig. 4D), which indicated that HOTAIRM1 could specifically bind to miR-30d-3p. Meanwhile, FISH data showed that HOTAIRM1 and miR-30d-3p evidently colocalized in the cytoplasm (Fig. 4E). miR-30d-3p expression was decreased following the overexpression of HOTAIRM1, while it was upregulated in the absence of HOTAIRM1 (Fig. 4F).

Additionally, the miR-30d-3p mimic reduced the luciferase activity of HSF1-WT without altering that of HSF1-MUT (Fig. 4G), demonstrating the specific binding between miR-30d-3p and HSF1. Furthermore, RT–qPCR results confirmed downregulated HSF1 expression following miR-30d-3p overexpression, while the opposite result was found upon miR-30d-3p inhibition (Fig. 4H). These findings demonstrated that HOTAIRM1 could attenuate the binding of miR-30d-3p to HSF1 by competitively binding to miR-30d-3p, thus enhancing the expression of HSF1.

HOTAIRM1 facilitates the proliferation and transdifferentiation of LFs through the miR-30d-3p/YY1/HSF1 axis

The aforementioned results allowed us to determine whether HOTAIRM1 induces the proliferation and transdifferentiation of LFs through the miR-30d-3p/YY1/HSF1 axis. The expression levels of HOTAIRM1, miR-30d-3p, YY1 and HSF1 were detected by RT–qPCR. There was no noticeable difference in the expression of HOTAIRM1, miR-30d-3p, YY1, and HSF1 between blank and oe-NC + sh-NC groups. Compared with the oe-NC + sh-NC group, HOTAIRM1, YY1, and HSF1 expression increased considerably and that of miR-30d-3p decreased markedly in the oe-HOTAIRM1 + sh-NC group. Compared with the oe-HOTAIRM1 + sh-NC group, the expression of HSF1 in the oe-HOTAIRM1 + sh-HSF1 group decreased sharply (Fig. 5A). The CCK-8 results illustrated that the proliferation of LFs treated with oe-HOTAIRM1 + sh-NC was increased, while it was repressed in the presence of oe-HOTAIRM1 + sh-HSF1 (Fig. 5B). Moreover, Western blot analysis and immunofluorescence assay results presented an increase in

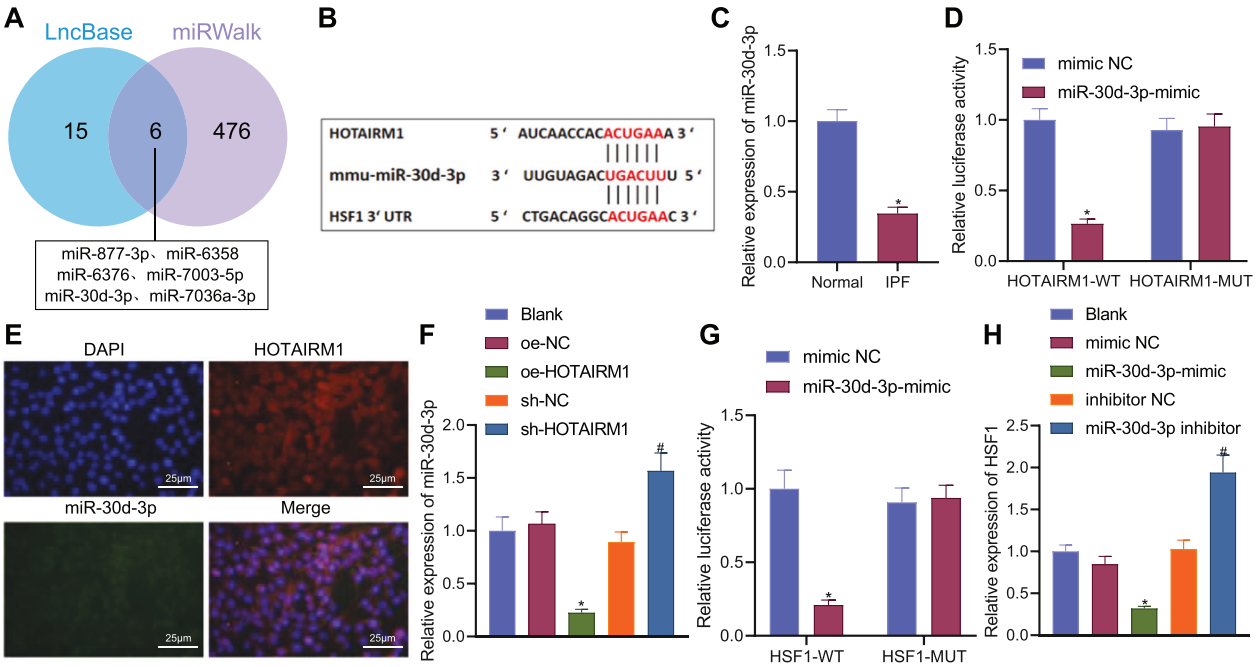

Fig. 4 HOTAIRM1 binds to miR-30d-3p and consequently increases the expression of the miR-30d-3p target HSF1. A Venn diagram of the predicted miRNAs binding to HOTAIRM1 and HSF1 by the LncBase and miRWalk databases. **B** Putative binding sites between miR-30d-3p and HOTAIRM1 and HSF1. **C** RT–qPCR detection of miR-30d-3p expression in the lung tissues of normal ($n = 6$) and IPF mice ($n = 6$). **D** Binding between HOTAIRM1 and miR-30d-3p confirmed by a dual-luciferase reporter assay in HEK-293T cells. **E** Subcellular colocalization of HOTAIRM1 and miR-30d-3p analyzed by FISH assay. **F** RT–qPCR detection of miR-30d-3p expression in the presence of oe-HOTAIRM1 or sh-HOTAIRM1. **G** Binding between HSF1 and miR-30d-3p confirmed by a dual-luciferase reporter assay in HEK-293T cells. **H** RT–qPCR detection of HSF1 expression in the presence of miR-30d-3p mimic or miR-30d-3p inhibitor. The data are shown as the mean ± standard deviation of three technical replicates. Data between two groups were analyzed by unpaired *t test*, while those among multiple groups were assessed by one-way ANOVA with Tukey's post-hoc tests. $^{*}p < 0.05$, compared with normal mice or treatment with mimic NC or oe-NC. $^{\#}p < 0.05$, compared with treatment with sh-NC or inhibitor NC.

the expression of α-SMA, collagen I, fibronectin, Ki67, and PCNA in the LFs treated with oe-HOTAIRM1 + sh-NC, which was reversed by treatment with oe-HOTAIRM1 + sh-HSF1 (Fig. 5C, D). Overall, the aforementioned data revealed that HOTAIRM1 increased the proliferation and transdifferentiation of LFs by mediating the miR-30d-3p/YY1/HSF1 axis.

Exosome-HOTAIRM1 promotes extracellular matrix remodeling in IPF mice through the miR-30d-3p/YY1/HSF1 axis

To further confirm the mechanism by which exosome-HOTAIRM1 regulates IPF progression in vivo, we overexpressed HOTAIRM1 in ACEs under normoxic conditions, extracted exosomes, and then injected exosomes and lentivirus into IPF mice *via* the tail vein. RT–qPCR results showed elevated expression trends of HOTAIRM1, YY1, and HSF1 and reduced miR-30d-3p levels in the lung tissues of mice with IPF. No notable difference was observed regarding the expression of these factors in IPF mice after treatment with exosomes-oe-NC + sh-NC. Relative to treatment with exosomes-oe-NC + sh-NC, exosomes-oe-HOTAIRM1 + sh-NC led to the higher expression of YY1 and HSF1 but lower miR-30d-3p expression. In contrast to exosomes-oe-HOTAIRM1 + sh-NC, YY1 expression was increased, but HSF1 expression was diminished after treatment with exosomes-oe-HOTAIRM1 + sh-HSF1 (Fig. 6A).

HE and Masson's trichrome staining data displayed evident inflammatory cell infiltration and capillary hyperplasia, increased collagen fiber bundles and lung fibrosis in the lung tissues of IPF-induced mice and those treated with exosomes-oe-NC + sh-NC. Moreover, lung tissue pathology and fibrosis were aggravated by the delivery of increased HOTAIRM1 by exosomes, which was undermined after silencing HSF1 (Supplementary Fig. 3A, B). As shown in Supplementary Fig. 3C and Fig. 6B, the lung tissues of IPF mice treated with exosomes-oe-NC + sh-NC presented similar changes in the expression of α-SMA, collagen I and fibronectin compared with nontreated IPF mice. A more evident increase was produced by exosomes-oe-HOTAIRM1 + sh-NC, but sh-HSF1 reversed this increase. The hydroxyproline level was similar in the lung tissues of nontreated IPF mice and those treated with exosomes-oe-NC + sh-NC. exosomes-oe-HOTAIRM1 + sh-NC led to higher hydroxyproline levels than exosomes-oe-NC + sh-NC. Conversely, this increase was abolished by HSF1 silencing (Fig. 6C).

IPF mice and those treated with exosomes-oe-NC + sh-NC showed similar lung compliance and lung resistance. Exosomes-oe-HOTAIRM1 + sh-NC induced a reduction in lung compliance and an increase in lung resistance. However, the opposite results were observed in response to treatment with exosomes-oe-HOTAIRM1 + sh-HSF1 (Fig. 6D). Taken together, these lines of evidence indicated that exosomes-HOTAIRM1 induced extracellular matrix remodeling in IPF mice through the miR-30d-3p/YY1/HSF1 axis.

DISCUSSION

Exosomes have been developed as therapeutic agents in multiple disease models, as exosomes derived from various types of cells can transfer distinct RNA profiles between cells [6]. The key findings attained from this study addressed the accelerating effect of HOTAIRM1 encapsulated by AEC-exosomes on IPF progression by controlling the miR-30d-3p/HSF1/YY1 axis.

It has been reported that profound pulmonary fibrosis is accompanied by a dramatic decrease in lung compliance and an increase in lung airway resistance [16]. Our initial results provided evidence suggesting that HOTAIRM1 was upregulated in the lung tissues of IPF mice and potentially contributed to the development and progression of IPF, as evidenced by reduced lung

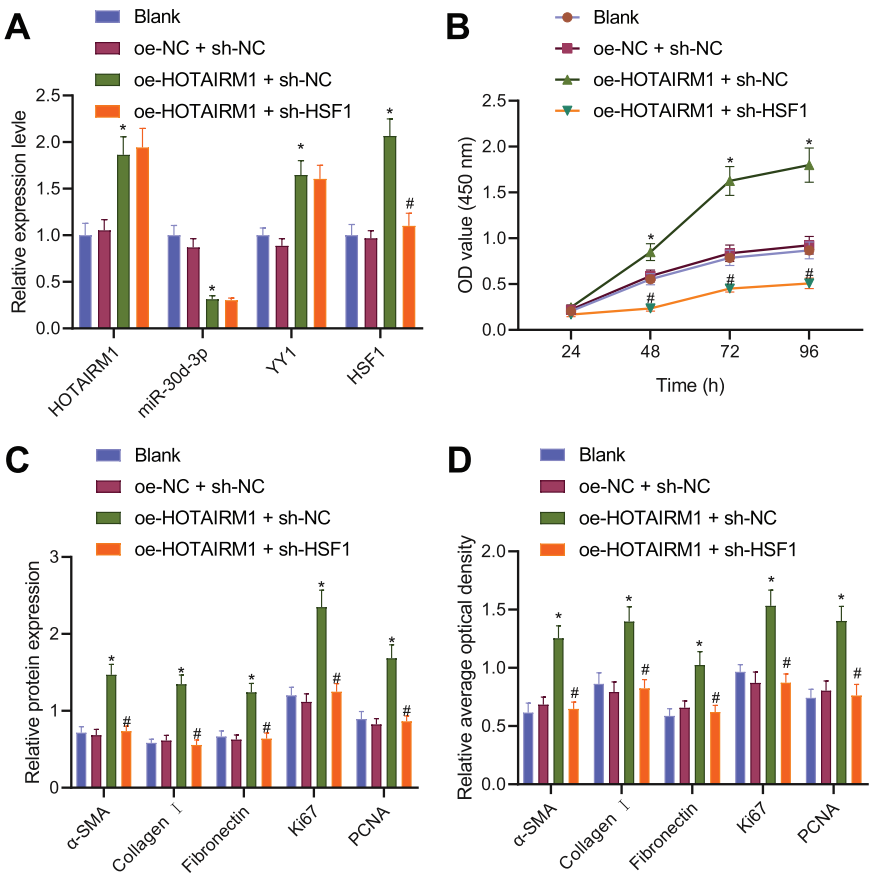

Fig. 5 HOTAIRM1 enhances the proliferation and transdifferentiation of LFs through the miR-30d-3p/YY1/HSF1 axis. A RT–qPCR detection of HOTAIRM1, YY1, HSF1, and miR-30d-3p expression in LFs treated with oe-HOTAIRM1 + sh-NC or oe-HOTAIRM1 + sh-HSF1. **B** CCK-8 detection of the proliferation of LFs treated with oe-HOTAIRM1 + sh-NC or oe-HOTAIRM1 + sh-HSF1. **C** Western blot analysis of α-SMA, collagen I, fibronectin, Ki67, and PCNA proteins in LFs treated with oe-HOTAIRM1 + sh-NC or oe-HOTAIRM1 + sh-HSF1. **D** Immunofluorescence analysis of α-SMA, collagen I, fibronectin, Ki67, and PCNA proteins in LFs treated with oe-HOTAIRM1 + sh-NC or oe-HOTAIRM1 + sh-HSF1. The data are shown as the mean ± standard deviation of three technical replicates. Data among multiple groups were assessed by one-way ANOVA with Tukey's post-hoc tests. Repeated measures ANOVA with Tukey's post-hoc test was applied for the comparison of data at different time points. $^{*}p < 0.05$, compared with treatment with oe-NC + sh-NC. $^{\#}p < 0.05$, compared with treatment with oe-HOTAIRM1 + sh-NC.

compliance and increased lung resistance and enhanced expression of fibrosis-related proteins α-SMA, collagen I and fibronectin as well as the level of hydroxyproline. A recent study has revealed that HOTAIRM1 knockdown leads to repressed cell viability, migration, invasion and glycolysis metabolism in NSCLC [17]. Recently, HOTAIRM1 has been regarded as a promoter of glucocorticoid resistance [18] and osteogenic differentiation [19]. The present results offer additional evidence for the role of HOTAIRM1 in IPF. HOTAIRM1 knockdown may have antifibrotic activity that may be considered in the treatment of IPF.

Our subsequent finding was that HOTAIRM1 could be delivered into LFs by AEC-exosomes, thereby promoting the proliferation and transdifferentiation of LFs. High HOTAIRM1 levels have been detected in exosomes, which can transfer HOTAIRM1 between parent cells and recipient cells [17, 20]. In addition, two-way communication between lung epithelial cells and LFs is responsible for the initiation of IPF [21]. Hypoxia can stimulate tubular epithelial cells to secrete exosomes and make exosomes to transfer RNA in the cell to promote the activation and proliferation of fibroblasts [22, 23]. The aforesaid information indicated that the promoting effect on the proliferation and transdifferentiation of LFs may be attributed to the transfer of HOTAIRM1 into LFs by AEC-exosomes.

Mechanistic investigations indicated that HOTAIRM1 recruited YY1 to activate HSF1 expression. Likewise, a number of studies have shown that lncRNAs can regulate the transcription of target genes by interacting with the transcription factor YY1 [24, 25]. Meanwhile, silencing YY1 reduces HSF1 expression, thus attenuating the expression of pro-proliferative and fibrosis markers in human embryonic pulmonary fibroblasts as well as repressing the proliferation and fibrogenic transformation of human embryonic pulmonary fibroblasts [15]. In partial agreement with this finding, our data highlighted the important role of HOTAIRM1-mediated YY1/HSF1 activation in the development of IPF and provided a reference for exploring new pathogenesis markers and biomarkers of IPF.

Increasing evidence has confirmed that HOTAIRM1 acts as a competing endogenous RNA of miRNAs, such as miR-107 and miR-106a-5p, and then regulates the expression of miRNA target genes [26, 27]. Here, this study demonstrated that HOTAIRM1 competitively bound to miR-30d-3p and consequently increased the expression of the miR-30d-3p target gene HSF1. It has been well established that miRNAs can interact with the 3′UTR of specific target mRNAs and consequently result in the inhibition of their expression [28]. The current study also represents the first evidence for the posttranscriptional regulation of HSF1 by miR-30d-3p, which may have important implications in regulating IPF progression. miR-30d expression is downregulated in PF tissues, but its overexpression attenuates TGF-β1-induced primary normal human LF proliferation and differentiation, as well as the protein levels of α-SMA and collagen I [29]. Notably, PF is considered to be a consequence of aberrant wound healing that induces fibroblast accumulation, differentiation and activation, and deposition of

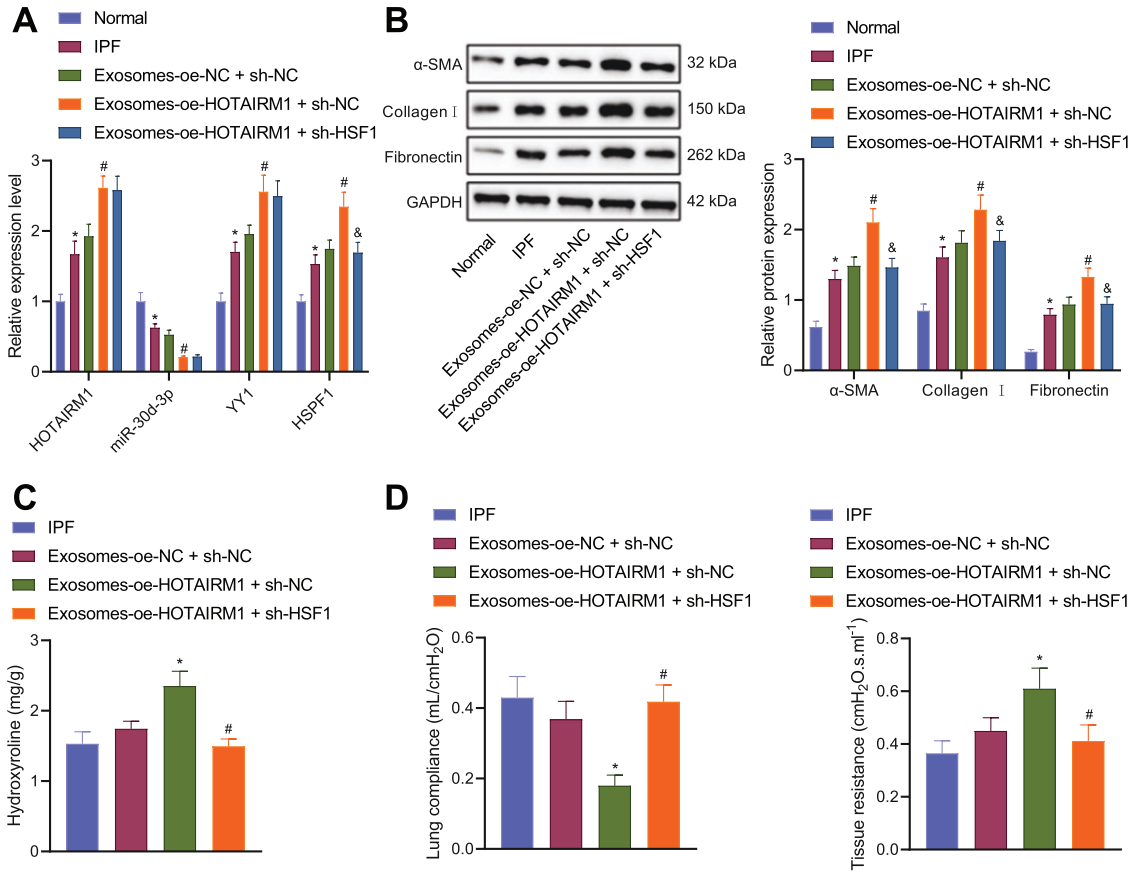

Fig. 6 Exos-HOTAIRM1 contributes to extracellular matrix remodeling in IPF mice through the miR-30d-3p/YY1/HSF1 axis. A RT–qPCR detection of HOTAIRM1, YY1, HSF1 and miR-30d-3p expression in the lung tissue of IPF mice and those treated with Exos-oe-HOTAIRM1 + sh-NC or Exos-oe-HOTAIRM1 + sh-HSF1. **B** Western blot analysis of α-SMA, collagen I, and fibronectin proteins in lung tissues of IPF mice and those treated with Exos-oe-HOTAIRM1 + sh-NC or Exos-oe-HOTAIRM1 + sh-HSF1. **C** Level of hydroxyproline in the lung tissue of IPF mice and those treated with Exos-oe-HOTAIRM1 + sh-NC or Exos-oe-HOTAIRM1 + sh-HSF1. **D** Lung compliance and resistance in the lung tissue of IPF mice and those treated with Exos-oe-HOTAIRM1 + sh-NC or Exos-oe-HOTAIRM1 + sh-HSF1. $n = 6$ for mice upon each treatment. The data are shown as the mean ± standard deviation. Data among multiple groups were assessed by one-way ANOVA with Tukey's post-hoc tests. $^{*}p < 0.05$, compared with normal mice or IPF mice treated with Exos-oe-NC + sh-NC. $^{\#}p < 0.05$, compared with IPF mice treated with Exos-oe-NC + sh-NC or Exos-oe-HOTAIRM1 + sh-NC. $^{\&}p < 0.05$, compared with IPF mice treated with Exos-oe-HOTAIRM1 + sh-NC.

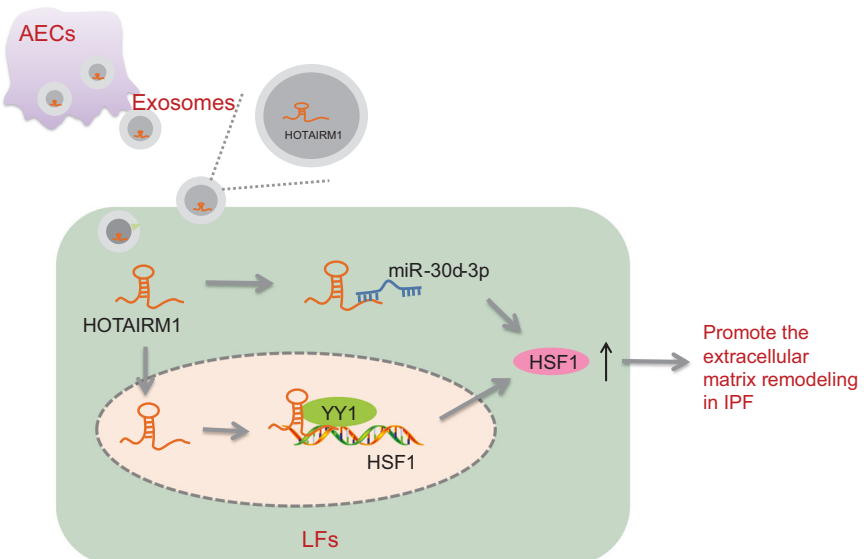

Fig. 7 Schematic diagram of the mechanism by which HOTAIRM1 delivered by AEC-Exos affects the extracellular matrix remodeling of IPF. HOTAIRM1 shuttled by Exos from hypoxia-induced AECs in LFs competitively binds to miR-30d-3p and recruits YY1 to upregulate HSF1, thereby promoting extracellular matrix remodeling of IPF.

excessive extracellular matrix components, in particular, collagen [30, 31]. In combination with the current results that exosomes-HOTAIRM1 facilitated the proliferation and transdifferentiation of LFs as well as extracellular matrix remodeling through the miR-30d-3p/YY1/HSF1 axis, HOTAIRM1 shuttled by AEC-exosomes may exert critical effects on the development and progression of IPF through the miR-30d-3p/YY1/HSF1 axis.

In summary, the data from our study support the notion that AEC exosomes transfer HOTAIRM1 from hypoxia-induced AECs into LFs, wherein HOTAIRM1 competitively binds to miR-30d-3p and recruits YY1 to upregulate HSF1, thereby promoting extracellular matrix remodeling of IPF (Fig. 7). Thus, our findings provide new insights into the mechanism of IPF progression and represent a novel strategy against IPF. Owing to the scarcity of literature concerning the interaction between HOTAIRM1 and miR-30d-3p, YY1, and HSF1, additional studies are required to validate the findings of the current study.

DATA AVAILABILITY

The data and materials of the study can be obtained from the corresponding author upon request.

REFERENCES

1. Antoniou, K. M., Margaritopoulos, G. A., Tomassetti, S., Bonella, F., Costabel, U. & Poletti, V. Interstitial lung disease. *Eur. Respir. Rev*. **23**, 40–54 (2014).
2. Meyer, K. C. Pulmonary fibrosis, part I: epidemiology, pathogenesis, and diagnosis. *Expert Rev. Respir. Med.* **11**, 343–359 (2017).
3. Sgalla, G., Kulkarni, T., Antin-Ozerkis, D., Thannickal, V. J. & Richeldi, L. Update in Pulmonary Fibrosis 2018. *Am. J. Respir. Crit. Care Med*. **200**, 292–300 (2019).
4. Chioma, O. S. & Drake, W. P. Role of microbial agents in pulmonary fibrosis. *Yale J. Biol. Med.* **90**, 219–227 (2017).
5. Mathai, S. K. & Schwartz, D. A. Translational research in pulmonary fibrosis. *Transl. Res.* **209**, 1–13 (2019).
6. Pegtel, D. M. & Gould, S. J. Exosomes. *Annu. Rev. Biochem*. **88**, 487–514 (2019).
7. Poulet C, Njock MS, Moermans C, Louis E, Louis R, Malaise M, et al. Exosomal long non-coding RNAs in lung diseases. *Int. J. Mol. Sci.* **21**, 3580–3635 (2020).
8. Cao, G., Zhang, J., Wang, M., Song, X., Liu, W. & Mao, C. et al. Differential expression of long non-coding RNAs in bleomycin-induced lung fibrosis. *Int. J. Mol. Med*. **32**, 355–364 (2013).
9. Bhan, A., Soleimani, M. & Mandal, S. S. Long noncoding RNA and cancer: a new paradigm. *Cancer Res* **77**, 3965–3981 (2017).
10. Xiong, F., Yin, H., Zhang, H., Zhu, C., Zhang, B. & Chen, S. et al. Clinicopathologic features and the prognostic implications of long noncoding RNA HOTAIRM1 in non-small cell lung cancer. *Genet. Test Mol. Biomarkers* **24**, 47–53 (2020).
11. Tanwar, V. S., Zhang, X., Jagannathan, L., Jose, C. C. & Cuddapah, S. Cadmium exposure upregulates SNAIL through miR-30 repression in human lung epithelial cells. *Toxicol Appl. Pharmacol.* **373**, 1–9 (2019).
12. Yang, C., Zhang, J. J., Peng, Y. P., Zhu, Y., Yin, L. D. & Wei, J. S. et al. A Yin-Yang 1/miR-30a regulatory circuit modulates autophagy in pancreatic cancer cells. *J. Transl. Med.* **15**, 211 (2017).
13. Zhang, C., Zhu, X., Hua, Y., Zhao, Q., Wang, K. & Zhen, L. et al. YY1 mediates TGF-beta1-induced EMT and pro-fibrogenesis in alveolar epithelial cells. *Respir Res.* **20**, 249 (2019).
14. Yang, W., Feng, B., Meng, Y., Wang, J., Geng, B. & Cui, Q. et al. FAM3C-YY1 axis is essential for TGFbeta-promoted proliferation and migration of human breast cancer MDA-MB-231 cells via the activation of HSF1. *J. Cell Mol. Med.* **23**, 3464–3475 (2019).
15. Chen, L., Yang, Y., Peng, X., Yan, H., Zhang, X. & Yin, L. et al. Transcription factor YY1 inhibits the expression of THY1 to promote interstitial pulmonary fibrosis by activating the HSF1/miR-214 axis. *Aging* **12**, 8339–8351 (2020).
16. Liu, X., Yang, L., Kwak, D., Hou, L., Shang, R. & Meyer, C. et al. Profound increase of lung airway resistance in heart failure: a potential important contributor for dyspnea. *J. Cardiovasc. Transl. Res.* **12**, 271–279 (2019).
17. Chen, D., Li, Y., Wang, Y. & Xu, J. LncRNA HOTAIRM1 knockdown inhibits cell glycolysis metabolism and tumor progression by miR-498/ABCE1 axis in non-small cell lung cancer. *Genes Genom* **43**, 183–194 (2021).
18. Liang, L., Gu, W., Li, M., Gao, R., Zhang, X. & Guo, C. et al. The long noncoding RNA HOTAIRM1 controlled by AML1 enhances glucocorticoid resistance by activating RHOA/ROCK1 pathway through suppressing ARHGAP18. *Cell Death Dis.* **12**, 702 (2021).
19. Ren, Y., Zhang, K., Wang, J., Meng, X., Du, X. & Shi, Z. et al. HOTAIRM1 promotes osteogenic differentiation and alleviates osteoclast differentiation by inactivating the NF-kappaB pathway. *Acta Bioch Bioph Sin* **53**, 201–211 (2021).
20. Alkhateeb T, Bah I, Kumbhare A, Youssef D, Yao ZQ, McCall CE, et al. Long non-coding RNA hotairm1 promotes S100A9 support of MDSC expansion during sepsis. *J. Clin. Cell Immunol*, **11**, 600 (2020).
21. Sakai, N. & Tager, A. M. Fibrosis of two: Epithelial cell-fibroblast interactions in pulmonary fibrosis. *Biochim. Biophys. Acta* **1832**, 911–921 (2013).
22. Guan, H., Peng, R., Mao, L., Fang, F., Xu, B. & Chen, M. Injured tubular epithelial cells activate fibroblasts to promote kidney fibrosis through miR-150-containing exosomes. *Exp Cell Res*. **392**, 112007 (2020).
23. Wang, W., Han, Y., Jo, H. A., Lee, J. & Song, Y. S. Non-coding RNAs shuttled via exosomes reshape the hypoxic tumor microenvironment. *J. Hematol. Oncol.* **13**, 67 (2020).
24. Han, X., Jiang, H., Qi, J., Li, J., Yang, J. & Tian, Y. et al. Novel lncRNA UPLA1 mediates tumorigenesis and prognosis in lung adenocarcinoma. *Cell Death Dis*. **11**, 999 (2020).
25. Song, S., Wang, Z., Li, Y., Ma, L., Jin, J. & Scott, A. W. et al. PPARdelta interacts with the hippo coactivator YAP1 to promote SOX9 expression and gastric cancer progression. *Mol. Cancer Res*. **18**, 390–402 (2020).
26. Li, D., Chai, L., Yu, X., Song, Y., Zhu, X. & Fan, S. et al. The HOTAIRM1/miR-107/TDG axis regulates papillary thyroid cancer cell proliferation and invasion. *Cell Death Dis*. **11**, 227 (2020).
27. Chao, H., Zhang, M., Hou, H., Zhang, Z. & Li, N. HOTAIRM1 suppresses cell proliferation and invasion in ovarian cancer through facilitating ARHGAP24 expression by sponging miR-106a-5p. *Life Sci*. **243**, 117296 (2020).
28. Ali Syeda Z, Langden SSS, Munkhzul C, Lee M, Song SJ. Regulatory mechanism of MicroRNA expression in cancer. *Int. J. Mol. Sci.* **21**, 1723 (2020).
29. Zhao, S., Xiao, X., Sun, S., Li, D., Wang, W. & Fu, Y. et al. MicroRNA-30d/JAG1 axis modulates pulmonary fibrosis through Notch signaling pathway. *Pathol Res. Pract.* **214**, 1315–1323 (2018).
30. Deng, Z., Fear, M. W., Suk Choi, Y., Wood, F. M., Allahham, A. & Mutsaers, S. E. et al. The extracellular matrix and mechanotransduction in pulmonary fibrosis. *Int. J. Biochem. Cell Biol.* **126**, 105802 (2020).
31. Kolahian, S., Fernandez, I. E., Eickelberg, O. & Hartl, D. Immune mechanisms in pulmonary fibrosis. *Am. J. Respir. Cell Mol. Biol.* **55**, 309–322 (2016).

AUTHOR CONTRIBUTIONS

L.C., Y.Y., and R.Y. designed the study. X.P., H.Y., and X.H. collated the data, carried out data analyses and produced the initial draft of the manuscript. L.C. and Y.Y. contributed to drafting the manuscript. All authors have read and approved the final submitted manuscript.

FUNDING

This work is supported by Project of Sichuan Provincial Department of Science and Technology 2021YFS0373).

COMPETING INTERESTS

The authors declare no competing interests.

ETHICS APPROVAL/CONSENT TO PARTICIPATE

This study was performed with the approval of the Animal Ethics Committee of Sichuan Provincial People's Hospital (2019047 A) and conformed to the Guide for the Care and Use of Laboratory Animals of the National Institutes of Health. Extensive efforts were made to minimize animal suffering.

ADDITIONAL INFORMATION

Supplementary information The online version contains supplementary material available at https://doi.org/10.1038/s41374-022-00782-y.

Correspondence and requests for materials should be addressed to XiaoBo Huang.

Reprints and permission information is available at http://www.nature.com/reprints

Publisher's note Springer Nature remains neutral with regard to jurisdictional claims in published maps and institutional affiliations.